RSC Advances

PAPER

View Article Online
View Journal | View Issue

Cite this: *RSC Adv.*, 2021, **11**, 39262

Electrochemical capacitive performance of thermally evaporated Al-doped CuI thin films

Nurhan Ghazal,[a] Metwally Madkour, *[b] Ahmed Abdel Nazeer, *[c] S. S. A. Obayya[a] and Shaimaa A. Mohamed[ade]

In this paper, we studied the electrochemical capacitive performance of thermally evaporated copper iodide thin film doped with different quantities of Al (3, 5, 7, and 9 mol%). The morphological structure, crystalline nature, and surface composition of the deposited films with different dopant levels were confirmed using X-ray powder diffraction (XRD), X-ray photoelectron spectroscopy (XPS), and field-emission scanning electron microscopy (FE-SEM). The electrochemical performance was evaluated based on cyclic voltammetry (CV), galvanostatic charge–discharge (GCD) measurements, and electrochemical impedance spectroscopy (EIS) in a Na_2SO_4 electrolyte. The XRD results confirm that the film is crystalline and has a face-centered cubic structure. The SEM images revealed trihedral-tipped structures with irregular nanocubes. The presence of the trihedral-tipped structures is more obvious in the Al-doped CuI films than in the bare film. We report a progressive increase in the specific capacitance values as the aluminum content increases, from 91.5 F g^{-1} for the pure CuI film to 108.3, 126.2, 142.8, and 131.1 F g^{-1} for the films with aluminum content of 3, 5, 7, and 9 mol%, respectively at a scan rate of 2 mV s^{-1}. The optimized CuI-Al electrode with 7 mol% aluminum content showed remarkable long-term cycling stability with 89.1% capacitance retention after 2000 charge/discharge cycles. Such a high performance for the CuI-7Al film as a supercapacitor can be ascribed to the aluminum doping, which increases the electrochemically active area compared to the bare CuI film and is critical for electron exchange at the electrode/electrolyte interface. Therefore, we introduce CuI-Al as a viable option for supercapacitor applications because of its low-cost production, excellent electrochemical performance, and cycling stability.

Received 8th October 2021
Accepted 21st November 2021

DOI: 10.1039/d1ra07455e

rsc.li/rsc-advances

1. Introduction

The expected depletion of fossil fuels and the environmental effects of greenhouse gas emissions on the atmosphere have driven a growing demand worldwide for sustainable energy supplies.[1] Renewable energy sources, such as solar energy, hydroelectric energy, and wind energy, have become the most promising solution for resolving these issues.[2,3] Energy production should be combined with an efficient storage system to store energy and supply power on demand to the planet.[4,5] In this context, batteries and supercapacitors are considered to be the two leading electrochemical energy storage technologies.[6,7] Batteries have been used successfully in portable electronics and have high specific energies or densities to be able to store energy for later use. However, batteries that suffer from low power density and a short life cycle cannot be widely applied for use in electric and hybrid vehicles.[8] Supercapacitors are flourishing as energy storage devices and can overcome the limits that batteries have as they possess high power densities and rapid charge/discharge times and are low weight, low cost, and highly flexible.[9,10] However, some supercapacitors still suffer from poor energy densities and require improvement.

There are two types of supercapacitors that store electrical charge using different working mechanisms. The first type are those that have electrochemical double-layer capacitors (EDLC). This non-faradaic process depends on physical charge separation from an interface. The other type uses pseudo-capacitance, a faradaic process that occurs between an electrolyte and a redox-active metal oxide or organic moiety.[11,12]

The development of electrode materials for use as efficient supercapacitors for energy storage requires a superior material capable of successfully holding charge. Copper iodide is a p-

[a]*Centre for Photonics and Smart Materials, Zewail City of Science and Technology, October Gardens, 6th of October City, Giza, Egypt*

[b]*Chemistry Department, Faculty of Science, Kuwait University, P. O. Box 5969, Safat, 13060, Kuwait. E-mail: metwally.madkour@ku.edu.kw; Tel: +965 90942431*

[c]*Electrochemistry Laboratory, Physical Chemistry Department, National Research Centre, P.O. 12622, Dokki, Giza, Egypt. E-mail: anazeer_nrc@yahoo.com*

[d]*Center for Nanotechnology, Zewail City of Science and Technology, October Gardens, 6th of October, Giza, 12578, Egypt*

[e]*Nanotechnology and Nanoelectronics Engineering Program, University of Science and Technology, Zewail City of Science and Technology, October Gardens, 6th of October City, Giza, Egypt*

type material with a direct band gap of 3.1 eV at room temperature, giving it high transparency in the visible region. It is recognized as a nondegenerate semiconductor and has an exciton binding energy of 62 meV, high hole mobility (>40 $cm^2 V^{-1} s^{-1}$) but with limited conductivity values below 100 S cm^{-1}.[13] By using the right amount of iodine doping, the hole conductivity may be improved even further[14] whilst the electrical conductivity can be improved by utilizing metallic dopants.[15] Copper iodide films can be deposited *via* various physical and chemical techniques, including electrodeposition, pulsed laser deposition, sputtering, and vacuum evaporation.[15,16] The properties of copper iodide make it stand out as a promising material for many applications. It has been introduced as a versatile hole transport material in optoelectronic devices.[17] In supercapacitors, copper iodide thin-films prepared *via* a successive ionic layer adsorption and reaction (SILAR) method exhibited electrochemical capacitive behavior and demonstrated a specific capacitance of 93 F g^{-1}.[18] Further investigation by Chinnakutti *et al.* on the electrochemical behavior of CuI thin films prepared *via* a solid iodination process exhibited a specific capacitance of 43 mF cm^{-2} at 10 mV s^{-1}.[14] The addition of dopants has been proposed as a promising strategy for improving the electrochemical activity of supercapacitor electrodes through the improvement of their conductivity.[19] In this regard, aluminum is considered an especially valuable additive material. Hu *et al.* reported that Al-doped α-MnO_2 had good electrochemical behavior with a greater specific capacitance than bare α-MnO_2.[20] Moreover, Al-doped NiO nanosheet arrays grown on nickel foam surfaces exhibited improved specific capacitance, good cycling behavior, and excellent rate capability compared to undoped NiO nanoarrays.[21] Nkele *et al.* compared undoped CuI films with CuI films doped with either 3% of Al, Pb or Zn, prepared using the SILAR method, and found that the Zn–CuI film exhibited a specific capacitance of 116 F g^{-1} at 2 mV s^{-1}.[22]

Herein, we study the electrochemical performance of bare CuI and Al-doped CuI thin films and reveal the effect that varying the aluminum content has on capacitive performance and accordingly on the capability of using Al-doped CuI thin films as a material in supercapacitors. We conducted cyclic voltammetry (CV), galvanostatic charge–discharge (GCD) and electrochemical impedance spectroscopy (EIS) measurements and applied a three-electrode configuration in 0.1 M Na_2SO_4 electrolytic solution to analyze the CuI thin-film performance before and after doping with different aluminum content. We also report the potential of a material, CuI-7Al, as an electrode for supercapacitor devices. The CuI-7Al electrode showed a high specific capacitance of 142.8 F g^{-1} at 2 mV s^{-1}, as well as pronounced long-term cyclic stability with 89.1% capacitance retention after 2000 charge/discharge cycles. The achieved results are promising compared with related energy storage materials.

2. Experimental details

2.1 Chemicals

Copper(II) sulfate pentahydrate, potassium iodide, aluminum chloride hexahydrate, ethanol and sodium sulphate were obtained from Sigma-Aldrich and utilized without any purification.

2.2 Synthesis

We implemented a coprecipitation method to synthesize CuI powder. Solutions of copper sulfate pentahydrate ($CuSO_4 \cdot 5H_2O$, 0.124 M) and potassium iodide (KI, 0.4 M) are separately prepared in distilled water and mixed at 80 °C under continuous stirring until a reddish brown color was obtained. We collected the residue then cleaned it with distilled water and ethanol many times until the brown color turne to tan color. We left it to dry in the oven at 60 °C overnight before grinding it to a fine CuI powder. To achieve different doping ratios (3, 5, 7, and 9 mol%) of aluminum, $AlCl_3 \cdot 6H_2O$ at different concentrations (3, 5, 7, and 9 mM) was added to a mixed solution of $CuSO_4 \cdot 5H_2O$ and KI.

For the sake of brevity, the CuI samples with different Al contents of 3 mol%, 5 mol%, 7 mol%, and 9 mol% are referred to as CuI-3Al, CuI-5Al, CuI-7Al, and CuI-9Al, respectively.

2.3 CuI thin-film deposition

2.5 cm × 2 cm stainless-steel substrates were cleaned in an ultrasonic bath at 80 °C for 15 min, after being rinsed with deionized water followed by acetone and isopropyl alcohol, and were then dried with nitrogen gas. The substrates were then treated with oxygen plasma for 5 minutes prior to use. A thermal evaporation system (Kurt J. Lesker) was used under a pressure of 2×10^{-5} mbar. The boat to substrate distance was adjusted to be 20 cm. After reaching the right vacuum, we increased the current to 60 A within 3 minutes and kept it constant for 4–5 minutes. Once the constant rate was reached, the shutter was opened to start the deposition up to a nanometer film thickness. Scheme 1 depicts the experimental methods used in this study.

2.4 Characterization techniques

A Bruker D8 Advance X-ray powder diffractometer (XRD) was used to examine the diffraction patterns of the nanoparticles. A Thermo ESCALAB 250 Xi spectrometer was used for the X-ray photoelectron spectroscopy (XPS) measurements, which were referenced using a C1s peak at 284.6 eV. A Joel JEM 1230, operating at 120 kV, was used to conduct scanning electron microscopy (SEM) experiments.

2.5 Electrochemical measurements

A Potentiostat/Galvanostat model Gamry 3000 was used to test the electrochemical performance. We employed CV, GCD and EIS measurements in a three-electrode system with the CuI film coated on a stainless-steel substrate acting as the working electrode. A saturated calomel (SCE) and platinum foil electrode were used as reference and counter electrodes, respectively. A 0.1 M Na_2SO_4 electrolyte solution was used within the potential window (−1 to 1 V *vs.* SCE). Electrochemical impedance spectroscopy measurements were carried out at $E_{app} = 0.0$ V with an AC voltage of 5 mV over a frequency range of 0.01 Hz to 100 kHz.

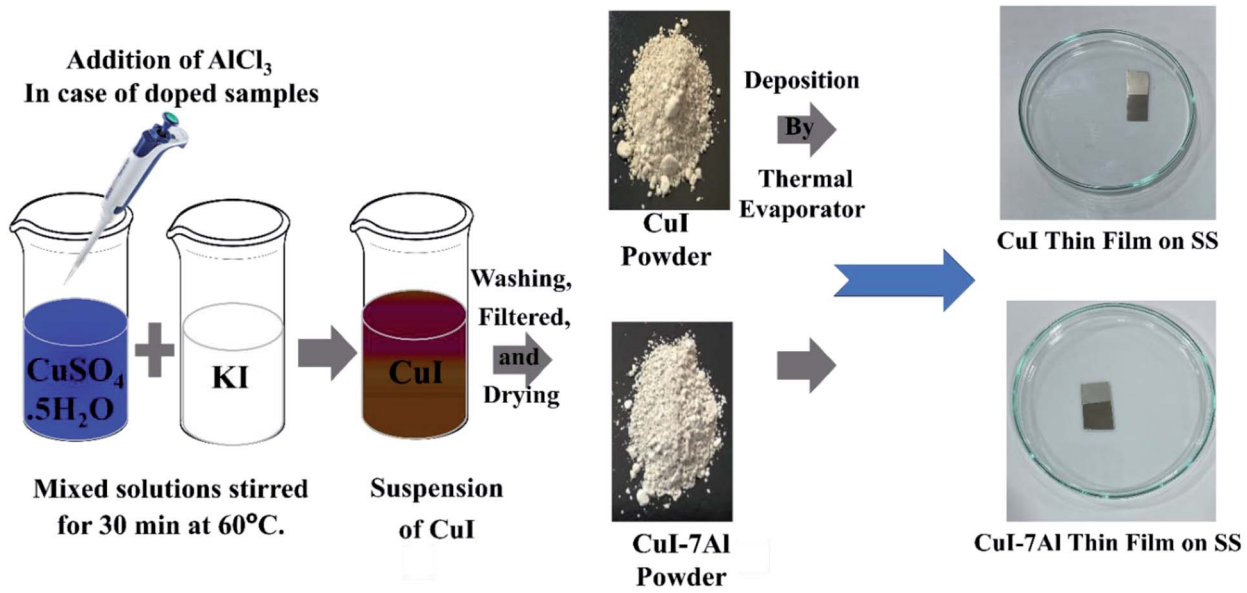

Scheme 1 Schematic diagram showing the preparation of the bare and Al-doped CuI thin films.

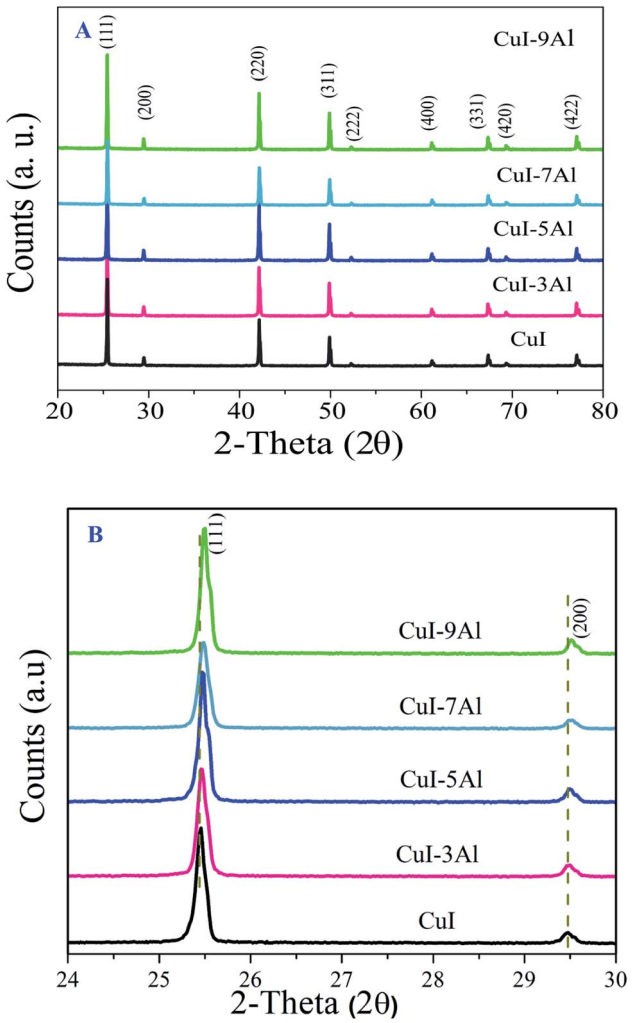

Fig. 1 (A) The XRD diffraction patterns for the bare and Al-doped CuI thin films. (B) Enlarged XRD patterns of the 24–30 2θ region.

3. Results and discussion

3.1 Characterization of the thin films

Fig. 1A shows the XRD patterns of the bare CuI thin films and those doped with different ratios of Al. The bare CuI film showed diffraction peaks at 25.5°, 29.5°, 42.2°, 49.9° 2θ which correspond to the (111), (200), (220), and (311) planes, respectively. This confirms the cubic crystal structure of CuI (DB card number 01-077-9398) which is consistent with previously reported results.[23]

The XRD patterns of the Al-doped CuI thin film samples are comparable to those of the bare samples, with no impurity phases. For the Al-doped CuI thin film samples, due to the reduced ionic radius of Al^{3+} (53 pm) compared to that of Cu^{+} (77 pm), the diffraction peaks showed a modest shift towards higher 2θ values (Fig. 1B) showing lattice compression which confirm the incorporation of the Al in the CuI lattice.[24]

Field-emission scanning electron microscopy (FE-SEM) images in Fig. 2 show the surface morphology of the bare and Al-doped CuI thin films. The films have structures with trihedral tips with relatively irregular and numerous nanocubes. The presence of the trihedral-tipped structures is more obvious in the Al-doped CuI films than in the bare CuI film. The introduction of Al dopants to the CuI film increased the number of trihedral tip clusters relative to the bare CuI film. This is could suggest that the surface energy of the Al-doped CuI films favors the agglomeration of grains resulting in the creation of larger trihedral-tipped clusters.[22]

To investigate the surface composition of the prepared films, XPS spectra of the bare and Al-doped CuI thin films were obtained and are presented in Fig. 3(a–d). For the Cu 2p spectrum in Fig. 3A, the peaks positioned at 951.9, and 932.1 eV are consistent with Cu $2p_{1/2}$ and Cu $2p_{3/2}$, respectively.[25] The disappearance of the satellite peaks proves that no Cu^{2+} is

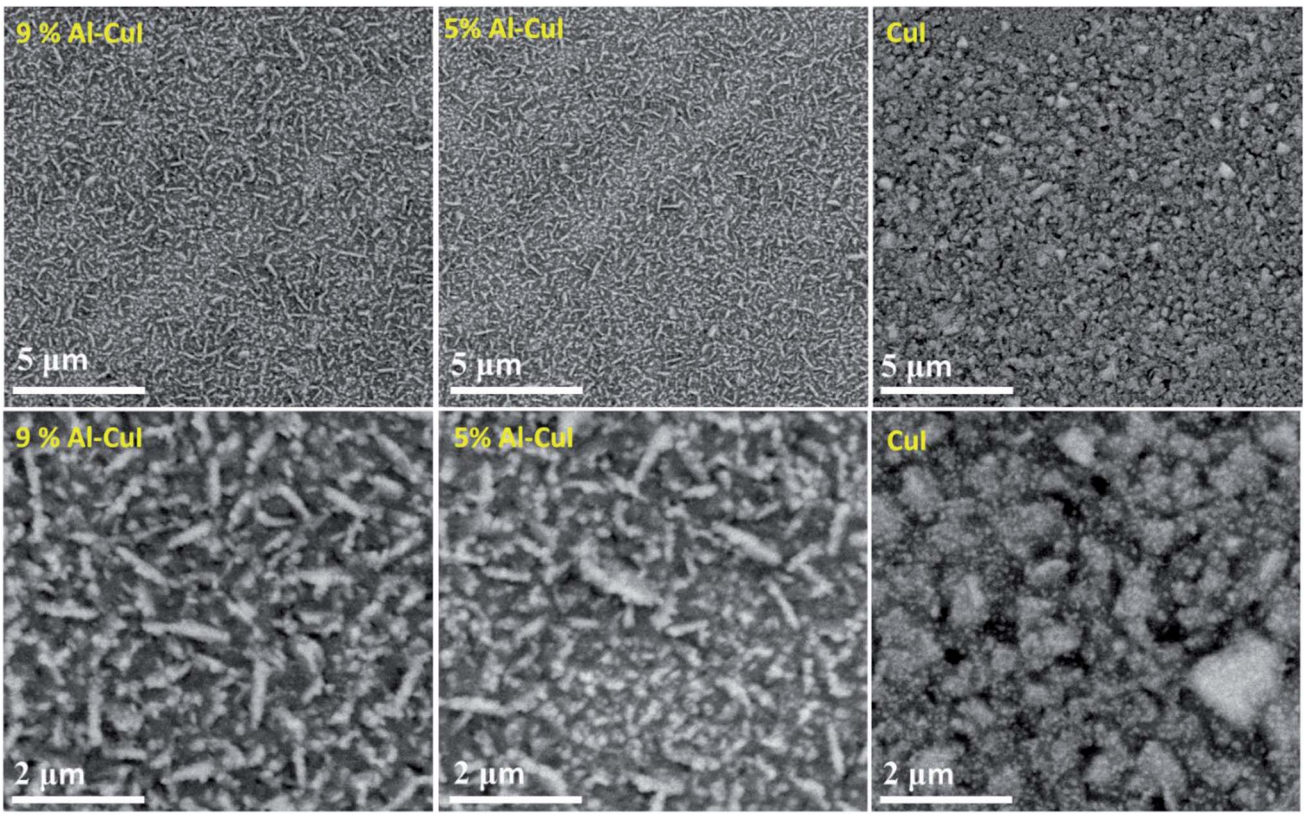

Fig. 2 FE-SEM images of the bare and Al-doped CuI thin films.

formed and only a single oxidation state, Cu^{1+}, is present.[26] The I 3d spectra (Fig. 3b) exhibited I 3d core levels at binding energies of 630 eV and 619 eV, which are attributed to 3d3/2 and 3d5/2, respectively.[27] Fig. 3c and d show the Cu 3p and Al 2p spectra with peaks at 73.23 eV and 75.54 eV ascribed to Al 2p and Cu 3p, respectively.

3.2 Electrochemical performance of the studied electrodes

A three-electrode configuration in 0.1 M Na_2SO_4 electrolytic solution was implemented to analyze the CuI thin-film performance before and after doping with different quantities of aluminum using the following electrochemical techniques.

3.2.1. Cyclic voltammetry (CV). Fig. 4a displays the cyclic voltammetry curves of the CuI-7Al electrode captured at various scan rates. The structure of the CV curves reveals the pseudocapacitive characteristics of the investigated electrodes depending on the oxidation and reduction peaks recorded. Furthermore, the CV curves retain their shape even after increasing the scan rate, which indicates excellent capacitive behavior and reversibility of these electrodes. According to the CV curves, it is obvious that the electrolyte ions adsorbed and collected on the surface of the examined electrodes resulted in their oxidation, followed by their reduction through the desorption reaction. The specific capacitance (C_{sp}) of the electrode was estimated from the CV results as follows:[28]

$$C_{sp} = \int (I\mathrm{d}V)/vmV \quad (1)$$

where I (A cm^{-2}) represents the current density, v (mV s^{-1}) is the scan rate, m (g) represents the mass of electroactive material, and V (V) represents the potential window. The specific capacitance values recorded, at a scan rate of 2 mV s^{-1} within the potential window of −1 to +1 V, for the investigated electrodes, CuI, CuI-3Al, CuI-5Al, CuI-7Al, CuI-9Al were 91.5, 108.3, 126.2, 142.8, 131.1 F g^{-1}, respectively.

The enhanced specific capacitances observed in the alumina-doped electrodes relative to the pristine CuI electrode arise from the large surface area, the large pore size for ion diffusion, better conductivity, and the higher electrochemical activity in aqueous solution. These properties support the penetration of electrolyte ions and enhance the charge storage characteristics of the examined materials. The CuI-7Al electrode showed a significant improvement in capacity relative to the pristine CuI owing to its higher porosity and surface area, which both enable easy and efficient access of both electrons and ions. Beyond this, increasing the Al dopant percentage to 9% resulted in a diminished capacity, which might be related to a decrease in the surface area. In the CV of CuI-7Al electrode, a higher scan rate results in a pronounced increase in the current plateau, suggesting that the fast and accessible ions in the electrolyte pass through its pores. Fig. 4b depicts the relationship between specific capacitance and scan rate. A significant drop in specific capacitance with increasing scan rate is seen with the best results for CuI-7Al.

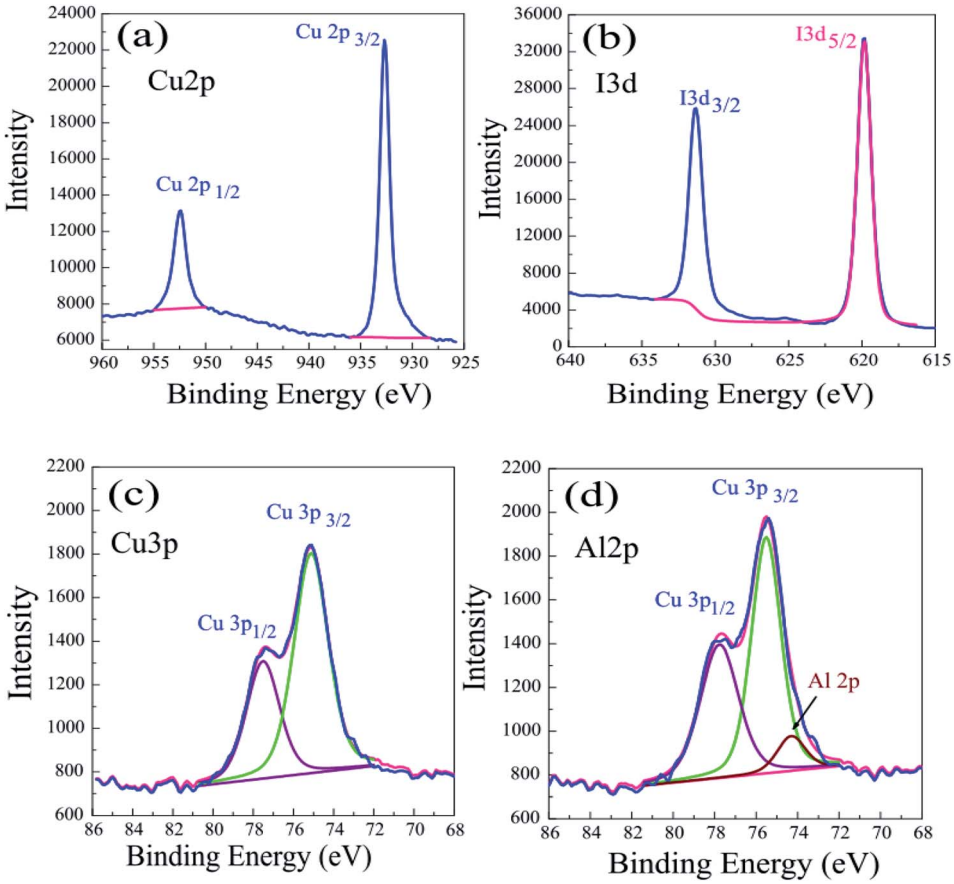

Fig. 3 XPS spectra of the bare and Al-doped CuI thin films. (a) XPS spectra of the Cu $2p_{3/2}$ and $2p_{1/2}$ regions. (b) XPS spectra of I 3d region. (c) XPS spectra of Cu 3p region. (d) XPS spectra of Cu 3P and Al 2p regions.

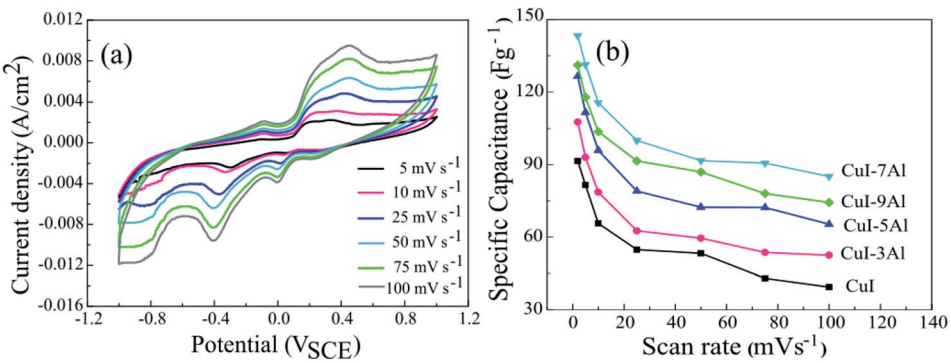

Fig. 4 (a) Cyclic voltammetry curves of CuI-7Al at different scan rates. (b) Specific capacitance *versus* scan rate for the bare and Al-doped CuI thin films.

3.2.2. Galvanostatic charge–discharge (GCD). Another essential criterion to be considered when assessing the performance of capacitive electrodes in energy applications is the rate capability, as appropriate electrodes have high specific capacitance at high charge rates.[29] To further clarify the enhanced electrochemical performance of the bare and Al-doped CuI thin-film electrodes, the GCD test was carried out using a three-electrode system in a Na_2SO_4 solution at different current densities over the potential range of −1.0 to +1.0 V/AgCl, as depicted in Fig. 5a. In this technique, the investigated electrode materials are subjected to sequential charging and discharging processes whilst monitoring the voltage response and estimating the specific capacitance from the slope of the discharge curve using the equation below:[30]

$$C_{sp} = (I\Delta t)/(m\Delta V) \quad (2)$$

where I represents the current density, t represents the discharge time, V represents the potential window, and m

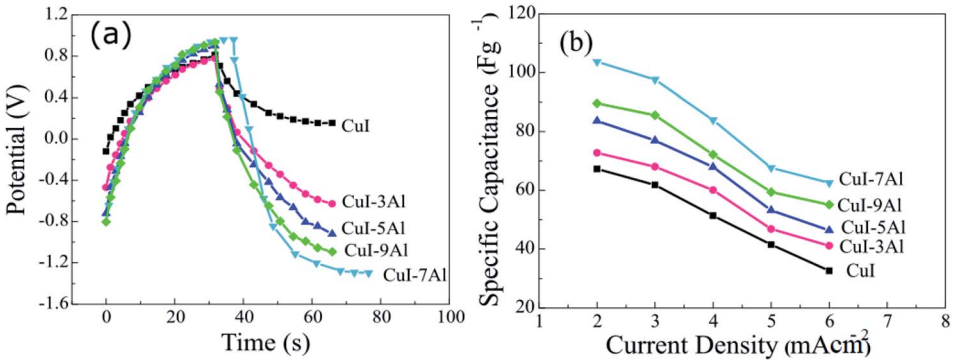

Fig. 5 (a) Galvanostatic charge–discharge comparison curves for the bare and Al-doped CuI thin films at 2 mA cm^{-2}. (b) The correlation of specific capacitance with current density for the bare and Al-doped CuI thin films.

represents the active mass of the material. Using this equation, the specific capacitance values recorded for the explored electrodes, CuI, CuI-3Al, CuI-5Al, CuI-7Al, and CuI-9Al, are 67.4, 72.7, 84.1.2, 103.4, and 89.6 F g^{-1}, respectively at a current density of 2 mA cm^{-2}. The CuI-7Al film shows the highest specific capacitance, the longest discharge time, and the lowest iR drop (voltage change across the electrochemical interface arising from uncompensated resistance), demonstrating a lower film resistance than the other electrodes. As shown in Fig. 5b, as the current density increases, the specific capacitance of the examined electrode material falls. The plateau region in the GCD curve is well-matched with the redox peak recorded in the cyclic voltammetry experiments, demonstrating the pseudocapacitive nature of the examined electrodes.

According to the results, and in agreement with the CV results, doping the CuI electrode with Al improved its electrochemical performance with the best results for CuI-7Al. Moreover, doping CuI with Al is believed to significantly increase its conductivity, which is vital for electron exchange at the electrode/electrolyte interface, resulting in higher pseudocapacitive behavior.

3.2.3. Electrochemical impedance spectroscopy (EIS). EIS was conducted over a frequency range of 0.01 Hz to 100 kHz to understand the electrochemical behaviors of the examined electrodes. The Nyquist plots of the investigated supercapacitor electrodes are shown in Fig. 6. From the figure, the electrodes show a similar shape with a straight line in the low-frequency region because of Warburg impedance and a semicircular form in the high-frequency region.[31] In harmony with the CV results, at low frequency, the CuI-7Al electrode had a more vertical slope than the bare CuI electrode or the other Al-doped CuI electrodes, demonstrating that the CuI-7Al electrode had a greater capacitive response, and lower diffusion resistance toward the electrolyte ions on the electrode surface.[32,33] Moreover, the Al-doped CuI electrodes had a shorter radius than the pristine CuI electrode at high frequency, suggesting better conductivity with rapid ion transport. The impedance characteristics were analyzed using the fitting circuit shown in the inset of Fig. 6. The charge transfer resistance (R_{ct}) between the electrode and electrolyte recorded for the Nyquist plots showed decreased electrode resistance for the Al-doped CuI electrodes,

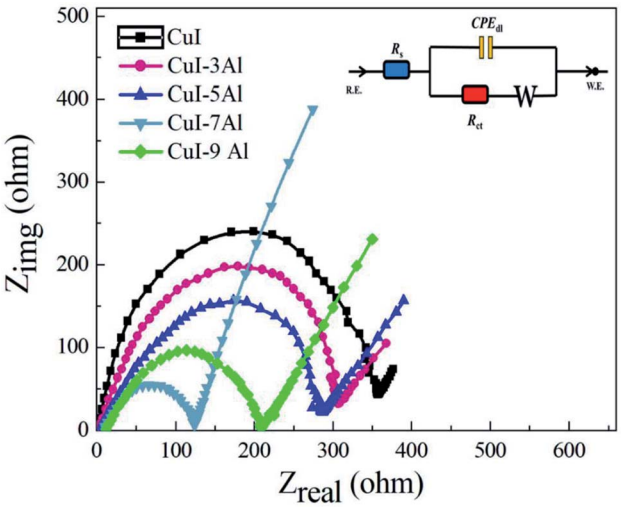

Fig. 6 Nyquist plots of the bare and Al-doped CuI thin films. The upper inset is the appropriate circuit used to fit the EIS results.

with the lowest R_{ct} recorded for the CuI-7Al electrode, demonstrating improved electronic and ionic conductivities.[21]

Furthermore, the improved specific capacitance of the Al-doped CuI electrodes could be because they have a larger electrochemically active area than the bare CuI, evidenced by the C_{dl} value recorded for the CuI-7Al electrode being the largest.

3.2.4. Galvanostatic charge–discharge cyclic stability. The long-term cycle stability and capacitance retention of the CuI-7Al-based supercapacitor electrode was assessed by measuring the capacitance fluctuation during 2000 charge/discharge cycles at 1.0 A g^{-1}. Fig. 7 shows that the CuI-7Al electrode has outstanding capacitive stability, which is standardized about the initial charge–discharge cycle. From this figure, an initial increase in capacitance was observed, which is probably because the electrical conditioning of the electrode surface makes it more susceptible to ion adsorption/desorption, followed by a slow decline in capacity retention after 2000 cycles to 89.1% of the initial value. The long-term cycle stability test requires redox reactions to occur over a long time period and the degradation of capacitance is believed to be due to possible

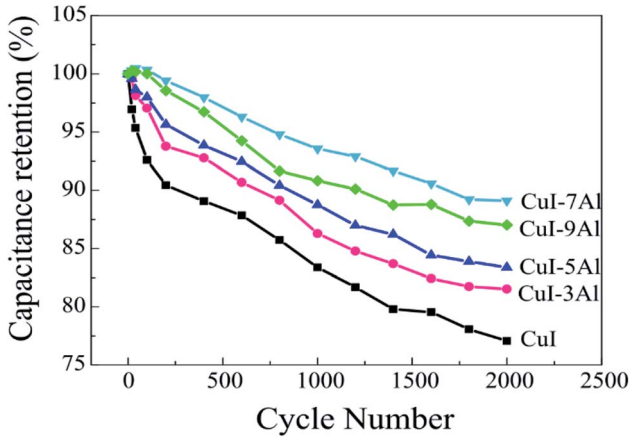

Fig. 7 Charge–discharge cyclic stability of the bare and Al-doped CuI thin films at a current density of 1 A g^{-1}.

destruction of the composition of the electrode. This may arise because of some quasi-reversible chemical reactions as well as the intercalation/deintercalation of electrolyte ions during charge–discharge cycles to counterbalance the overall charge resulting in a decrease in their performance. Moreover, the repeated charge–discharge process may cause mechanical and electrical problems, lowering the initial performance due to the loss of mass of the active material.

3.3 Performance discussion

The electrode materials employed in supercapacitors can be categorized into three major types according to their charge storage mechanism: (1) electric double layer materials, (2) pseudo-capacitors, and (3) battery-type materials.[34] Electrical charge can be stored on the electrode surface generating double layer charging (capacitive nature) or inside the bulk of the active material (non-capacitive nature).[35] Energy is stored in pseudo-capacitors *via* faradaic charge–transfer processes between the electrode materials and the ions of the electrolyte within the investigated voltage windows. In this work, the CuI-7Al electrode had excellent electrochemical performance when compared to the undoped CuI electrode, showing that doping CuI with Al results in enhanced performance. The enhanced specific capacitance of the CuI-doped Al electrode might originate from a larger electrochemically active area when compared with its undoped counterpart, as proven by the EIS measurements. The CuI-7Al electrode has a lower R_{ct} than the pure CuI electrode, implying that a synergistic effect between CuI and Al is responsible for the quick charge transfer on the electrode surface. The small semicircle in the high frequency area of the Nyquist plots depicts rapid charge movement between the electrode and electrolyte. The redox peaks of the CuI-7Al electrode material in Na_2SO_4 can be attributed to the intercalation/de-intercalation of Na^+ ions into/from the CuI-7Al electrode lattice. The porous nature of the CuI-7Al film contributed to the better intercalation/de-intercalation of the ions, resulting in a high specific capacitance. CuI-7Al has a better capacitive performance because of the Al doping, which allows for faster electrode kinetics and diffusion than a bare CuI electrode. Furthermore, the large surface area of the electrode ensures more active centers, which guarantee effective redox reactions and rapid ion transport.

4. Conclusions

In summary, we present the preparation of CuI thin films doped with different weight percentages of Al (3, 5, 7, and 9 mol%) using a thermal evaporation technique to achieve an enhanced capacitive performance relative to a bare CuI film. Electrochemical studies reveal that the CuI-7Al thin film possesses lower charge transfer resistance, good cycle stability, and a specific capacitance of 142.8 F g^{-1} at a 2 mV s^{-1} scan rate. The enhanced specific capacitance of CuI-7Al can be ascribed to increased conductivity and a reduced charge transfer resistance, resulting in improved electrochemical performance of the Al-doped CuI material.

Conflicts of interest

There are no conflicts to declare.

Acknowledgements

The researchers acknowledge the support of the Research Administration at Kuwait University *via* RSPU, Facilities No. (GS 01/01, GS 01/05, GS 02/01, GE 01/07, GE 03/08 and GS 03/01).

References

1 S. Chu and A. Majumdar, Opportunities and challenges for a sustainable energy future, *Nature*, 2012, **488**, 294–303.
2 A. Hagfeldt, G. Boschloo, L. Sun, L. Kloo and H. Pettersson, Dye-Sensitized Solar Cells, *Chem. Rev.*, 2010, **110**, 6595–6663.
3 K. Christopher and R. Dimitrios, A review on exergy comparison of hydrogen production methods from renewable energy sources, *Energy Environ. Sci.*, 2012, **5**, 6640–6651.
4 Z. Yang, J. Zhang, M. C. W. Kintner-Meyer, X. Lu, D. Choi, J. P. Lemmon and J. Liu, Electrochemical Energy Storage for Green Grid, *Chem. Rev.*, 2011, **111**, 3577–3613.
5 H. Wang and H. Dai, Strongly coupled inorganic–nano-carbon hybrid materials for energy storage, *Chem. Soc. Rev.*, 2013, **42**, 3088–3113.
6 Y. Shao, M. F. El-Kady, J. Sun, Y. Li, Q. Zhang, M. Zhu, H. Wang, B. Dunn and R. B. Kaner, Design and Mechanisms of Asymmetric Supercapacitors, *Chem. Rev.*, 2018, **118**, 9233–9280.
7 A. A. Ali, A. A. Nazeer, M. Madkour, A. Bumajdad and F. Al Sagheer, Novel supercapacitor electrodes based semiconductor nanoheterostructure of CdS/rGO/CeO2 as efficient candidates, *Arabian J. Chem.*, 2018, **11**, 692–699.
8 V. Etacheri, R. Marom, R. Elazari, G. Salitra and D. Aurbach, Challenges in the development of advanced Li-ion batteries: a review, *Energy Environ. Sci.*, 2011, **4**, 3243–3262.

9 B. K. Kim, S. Sy, A. Yu and J. Zhang, Electrochemical Supercapacitors for Energy Storage and Conversion, *Handbook of Clean Energy Systems*, 2015, pp. 1–25.
10 C.-C. Hu, W.-C. Chen and K.-H. Chang, How to Achieve Maximum Utilization of Hydrous Ruthenium Oxide for Supercapacitors, *J. Electrochem. Soc.*, 2004, **151**, A281.
11 J. Wang, S. Dong, B. Ding, Y. Wang, X. Hao, H. Dou, Y. Xia and X. Zhang, Pseudocapacitive materials for electrochemical capacitors: from rational synthesis to capacitance optimization, *Natl. Sci. Rev.*, 2016, **4**, 71–90.
12 N. K. Mishra, R. Mondal and P. Singh, Synthesis, characterizations and electrochemical performances of anhydrous CoC2O4 nanorods for pseudocapacitive energy storage applications, *RSC Adv.*, 2021, **11**, 33926–33937.
13 C. Yang, M. Kneiβ, M. Lorenz and M. Grundmann, Room-temperature synthesized copper iodide thin film as degenerate p-type transparent conductor with a boosted figure of merit, *Proc. Natl. Acad. Sci. U. S. A.*, 2016, **113**, 12929–12933.
14 K. K. Chinnakutti, V. Panneerselvam, D. Govindarajan, A. k. Soman, K. Parasuraman and S. Thankaraj Salammal, Optoelectronic and electrochemical behaviour of γ-CuI thin films prepared by solid iodination process, *Prog. Nat. Sci.: Mater. Int.*, 2019, **29**, 533–540.
15 A. Liu, H. Zhu, M.-G. Kim, J. Kim and Y.-Y. Noh, Engineering Copper Iodide (CuI) for Multifunctional p-Type Transparent Semiconductors and Conductors, *Adv. Sci.*, 2021, **8**, 2100546.
16 P. M. Sirimanne, M. Rusop, T. Shirata, T. Soga and T. Jimbo, Characterization of CuI thin films prepared by different techniques, *Mater. Chem. Phys.*, 2003, **80**, 461–465.
17 W. Sun, H. Peng, Y. Li, W. Yan, Z. Liu, Z. Bian and C. Huang, Solution-Processed Copper Iodide as an Inexpensive and Effective Anode Buffer Layer for Polymer Solar Cells, *J. Phys. Chem. C*, 2014, **118**, 16806–16812.
18 B. N. Ezealigo, A. C. Nwanya, A. Simo, R. U. Osuji, R. Bucher, M. Maaza and F. I. Ezema, Optical and electrochemical capacitive properties of copper (I) iodide thin film deposited by SILAR method, *Arabian J. Chem.*, 2019, **12**, 5380–5391.
19 B. Li, M. Zheng, H. Xue and H. Pang, High performance electrochemical capacitor materials focusing on nickel based materials, *Inorg. Chem. Front.*, 2016, **3**, 175–202.
20 Z. Hu, X. Xiao, C. Chen, T. Li, L. Huang, C. Zhang, J. Su, L. Miao, J. Jiang, Y. Zhang and J. Zhou, Al-doped α-MnO2 for high mass-loading pseudocapacitor with excellent cycling stability, *Nano Energy*, 2015, **11**, 226–234.
21 J. Chen, X. Peng, L. Song, L. Zhang, X. Liu and J. Luo, Facile synthesis of Al-doped NiO nanosheet arrays for high-performance supercapacitors, *R. Soc. Open Sci.*, 2018, **5**, 180842.
22 A. C. Nkele, U. K. Chime, A. C. Nwanya, D. Obi, R. U. Osuji, R. Bucher, P. M. Ejikeme, M. Maaza and F. I. Ezema, Role of metallic dopants on the properties of copper (1) iodide nanopod-like structures, *Vacuum*, 2019, **161**, 306–313.
23 N. Salah, A. M. Abusorrah, Y. N. Salah, M. Almasoudi, N. Baghdadi, A. Alshahri and K. Koumoto, Effective dopants for CuI single nanocrystals as a promising room temperature thermoelectric material, *Ceram. Int.*, 2020, **46**, 27244–27253.
24 B. Poornaprakash, U. Chalapathi, S. V. P. Vattikuti, M. C. Sekhar, B. P. Reddy, P. T. Poojitha, M. S. P. Reddy, Y. Suh and S.-H. Park, Enhanced fluorescence efficiency and photocatalytic activity of ZnS quantum dots through Ga doping, *Ceram. Int.*, 2019, **45**, 2289–2294.
25 M. Kumar, V. Bhatt, O. S. Nayal, S. Sharma, V. Kumar, M. S. Thakur, N. Kumar, R. Bal, B. Singh and U. Sharma, CuI nanoparticles as recyclable heterogeneous catalysts for C–N bond formation reactions, *Catal. Sci. Technol.*, 2017, **7**, 2857–2864.
26 M. Madkour, CuxO thin films via ultrasonic spray pyrolysis as efficient solar photocatalysts: Single source polymeric coordinated precursor, *Colloid Interface Sci. Commun.*, 2021, **44**, 100497.
27 S. Lee, H. J. Lee, Y. Ji, S. M. Choi, K. H. Lee and K. Hong, Vacancy engineering of a solution processed CuI semiconductor: tuning the electrical properties of inorganic P-channel thin-film transistors, *J. Mater. Chem. C*, 2020, **8**, 9608–9614.
28 A. A. Nazeer, A. A. Husain, J. Samuel, N. Rajendran and S. Makhseed, Hydroxyl-functionalized microporous polymer for enhanced CO2 uptake and efficient super-capacitor energy storage, *React. Funct. Polym.*, 2020, **154**, 104670.
29 A. E. Rashed and A. A. El-Moneim, Two steps synthesis approach of MnO2/graphene nanoplates/graphite composite electrode for supercapacitor application, *Mater. Today Energy*, 2017, **3**, 24–31.
30 J. Jayachandiran, J. Yesuraj, M. Arivanandhan, B. Muthuraaman, R. Jayavel and D. Nedumaran, Bifunctional investigation of ultra-small SnO2 nanoparticle decorated rGO for ozone sensing and supercapacitor applications, *RSC Adv.*, 2021, **11**, 856–866.
31 X. Pan, Y. Zhao, G. Ren and Z. Fan, Highly conductive VO2 treated with hydrogen for supercapacitors, *Chem. Commun.*, 2013, **49**, 3943–3945.
32 M. D. Stoller, S. Park, Y. Zhu, J. An and R. S. Ruoff, Graphene-Based Ultracapacitors, *Nano Lett.*, 2008, **8**, 3498–3502.
33 Y. Lin, J. Li, P. Ren and X. Yang, NH4V4O10 nanobelts vertically grown on 3D TiN nanotube arrays as high-performance electrode materials of supercapacitors, *RSC Adv.*, 2021, **11**, 8468–8474.
34 Poonam, K. Sharma, A. Arora and S. K. Tripathi, Review of supercapacitors: Materials and devices, *J. Energy Storage*, 2019, **21**, 801–825.
35 A. Noori, M. F. El-Kady, M. S. Rahmanifar, R. B. Kaner and M. F. Mousavi, Towards establishing standard performance metrics for batteries, supercapacitors and beyond, *Chem. Soc. Rev.*, 2019, **48**, 1272–1341.